



**HAL**  
open science

## Precision calculation of low-energy electron-impact excitation cross sections of sodium

Xiang Gao, Xiao-Ying Han, Lan Voky, Nicole Feautrier, Jia-Ming Li

► **To cite this version:**

Xiang Gao, Xiao-Ying Han, Lan Voky, Nicole Feautrier, Jia-Ming Li. Precision calculation of low-energy electron-impact excitation cross sections of sodium. *Physical Review A*, 2010, 81, pp.22703. 10.1103/PhysRevA.81.022703 . hal-03784883

**HAL Id: hal-03784883**

**<https://hal.science/hal-03784883>**

Submitted on 29 Sep 2022

**HAL** is a multi-disciplinary open access archive for the deposit and dissemination of scientific research documents, whether they are published or not. The documents may come from teaching and research institutions in France or abroad, or from public or private research centers.

L'archive ouverte pluridisciplinaire **HAL**, est destinée au dépôt et à la diffusion de documents scientifiques de niveau recherche, publiés ou non, émanant des établissements d'enseignement et de recherche français ou étrangers, des laboratoires publics ou privés.

**Precision calculation of low-energy electron-impact excitation cross sections of sodium**Xiang Gao,<sup>1</sup> Xiao-Ying Han,<sup>2</sup> Lan Voky,<sup>4</sup> Nicole Feautrier,<sup>4</sup> and Jia-Ming Li<sup>1,3</sup><sup>1</sup>*Department of Physics, Shanghai Jiao Tong University, Shanghai 200240, People's Republic of China*<sup>2</sup>*The Key Laboratory of Computational Physics, Institute of Applied Physics and Computational Mathematics, Beijing 100088, People's Republic of China*<sup>3</sup>*Key Laboratory of Atomic and Molecular Nanosciences of Education Ministry, Department of Physics, Tsinghua University, Beijing 100084, People's Republic of China*<sup>4</sup>*LERMA, UMR 8112 du CNRS, Observatoire de Paris, 92915 Meudon Cedex, France*

(Received 24 August 2009; published 4 February 2010)

The collision cross sections of sodium from the ground state to the first four excited states at the incident energy ranging from 0 to 5.4 eV are calculated using the  $R$ -matrix method. The convergences of the cross sections are checked systematically by using four sets of high-quality target states, i.e., 5, 9, 14, and 19 physical target states. The influence of the Rydberg target states on the collision cross sections is also elucidated at higher incident energies; i.e., the amplitude of resonance structures will decrease with respect to the effective quantum number  $\nu$  of the Rydberg target states. This result is very useful for the calculations of these cross sections at intermediate energy with finite target states by combining the partial-wave-expansion methods valid at low energy with the first Born approximation method valid at high energy, which would be of great importance in obtaining complete cross-section data for related scientific fields.

DOI: [10.1103/PhysRevA.81.022703](https://doi.org/10.1103/PhysRevA.81.022703)

PACS number(s): 34.80.Dp, 31.15.A–, 31.15.vj

**I. INTRODUCTION**

The process of electron-impact excitation plays an important role in various fields, such as radiation physics [1], plasma physics [2], atmospheric physics [3], and astrophysics [3–5], in which the collision cross sections are the indispensable physical parameters. Since the 1930s, both experimental measurements and theoretical calculations have been carried out to obtain the electron collision cross sections of sodium owing to its relatively simple electronic structure (reviewed by Ref. [6,7]). For instance, Enemark and Gallagher measured the collision cross section for the strong transition  $3s-3p$  at a wide energy range; i.e., from threshold (2.1 eV) to 1000 eV [8]. The measurement of collision cross sections from the ground state to the final excited states (up to  $7f$ ) with the energy range of 0–150 eV was also reported [9]. However, due to the experimental difficulties, distinct differences exist between the collision cross sections obtained in the above two measurements, which reaches 50% even for the  $3p$  state. As for the theoretical calculations, apart from the Bethe or first Born approximation, calculations based on close-coupling method were also reported, e.g., four-state close coupling calculations [10] and coupled-channels  $R$ -matrix calculations with 11 target states [6]. But those theoretical calculations at low incident energies are still limited. The dynamical process in this energy region becomes very complicated when the resonance structures caused by including higher Rydberg target states are involved. Therefore, more complete and precision theoretical results are motivated. In this work, using the  $R$ -matrix method [11–17] we systematically calculated the collision cross sections of sodium from ground state to the first four excited states at incident energy ranging from 0 to 5.4 eV (above the  $3s$  ionization threshold) by four sets of high-quality target states; i.e., 5, 9, 14, and 19 physical target states, respectively. Our calculated cross sections are in good agreement with the available absolute experimental results [9].

At low incident energies, our calculated cross sections are in good agreement with the previous theoretical results [6]. At higher incident energies, the influence of such Rydberg target states to the collision cross sections is elucidated, i.e., the amplitude of resonance structures will decrease with respect to the effective quantum number  $\nu$  represented by the Rydberg target states considered. Therefore, for the cross sections of electron impact excitation between the lower excited targets, we only need to use finite physical target states in practical calculations. It implies that the cross sections obtained by the partial-wave expansion methods at low energy could be interfaced with the cross sections obtained by the first Born approximation method at high energy [18]. A scheme to calculate the cross sections in the entire incident energy range is discussed in the conclusions, which should be very important to obtain the complete cross-section data for related scientific fields.

**II. THEORETICAL METHODS AND CALCULATION RESULTS**

The detailed descriptions of  $R$ -matrix method dealing with the electron-atom collision process have been presented in the previous works [11–17]. Only a brief outline will be given here. This method begins by partitioning the subconfiguration space of the colliding electron into two regions by a sphere of radius  $a$  centered on the nucleus. In the external region  $r > a$ , where  $r$  is the distance of the colliding electron relative to the centroid of target (i.e., the atom), the exchange interactions between the colliding electron and the target electrons are negligible. The colliding electron mainly feels a “free potential” with approximate long-range static polarization potentials. Within the reaction zone  $r \leq a$ , the interactions between the colliding electron and the target electrons involve electron exchange and correlation interactions. It is a many-electron problem, which is solved variationally as a whole to obtain the logarithmic

TABLE I. The basis sets used in the calculations.

Basis set no.	Atomic orbitals (AO) <sup>a</sup>	Physical target states <sup>c</sup>	No. of physical target states	No. of other target states <sup>e</sup>	Configurations of ( $N + 1$ )-electron system in $R$ -matrix calculation <sup>f</sup>
Set 1	$v_2, v_3, \bar{v}_4^b$	$2p^6 3s^1 {}^2S^e, 2p^6 3p^1 {}^2P^o, 2p^6 4s^1 {}^2S^e,$ $2p^6 3d^1 {}^2D^e, 2p^6 4p^1 {}^2P^o$	5	26	$2p^6 AO^2, 2p^5 AO^3$
Set 2	$v_2, v_3, v_4, \bar{v}_5^b$	Set 1 <sup>d</sup> + $2p^6 5s^1 {}^2S^e, 2p^6 4d^1 {}^2D^e,$ $2p^6 4f^1 {}^2F^o, 2p^6 5p^1 {}^2P^o$	9	42	$2p^6 AO^2, 2p^5 AO^3$
Set 3	$v_2, v_3, v_4, v_5, \bar{v}_6^b$	Set 2 <sup>d</sup> + $2p^6 6s^1 {}^2S^e, 2p^6 5d^1 {}^2D^e,$ $2p^6 5f^1 {}^2F^o, 2p^6 5g^1 {}^2G^e, 2p^6 6p^1 {}^2P^o$	14	41	$2p^6 AO^2, 2p^5 AO^3$
Set 4	$v_2, v_3, v_4, v_5, v_6, \bar{v}_7^b$	Set 3 <sup>d</sup> + $2p^6 7s^1 {}^2S^e, 2p^6 6d^1 {}^2D^e,$ $2p^6 6f^1 {}^2F^o, 2p^6 6g^1 {}^2G^e, 2p^6 7p^1 {}^2P^o$	19	43	$2p^6 AO^2, 2p^5 AO^3$

<sup>a</sup>One-electron atomic orbitals used to construct the multielectron bases, including the spectroscopy orbital denoted as  $nl$  and polarized pseudo-orbitals denoted as  $n\bar{l}$ .

<sup>b</sup>Orbitals classified by manifold, denoted by:  $v_2 = 3s, 3p; v_3 = 4s, 3d, 4p; v_4 = 5s, 4d, 4f, 5p; \bar{v}_4 = 5\bar{s}, 4\bar{d}, 4\bar{f}, 5\bar{p}; v_5 = 6s, 5d, 5f, 5g, 6p; \bar{v}_5 = 6\bar{s}, 5\bar{d}, 5\bar{f}, 5\bar{g}, 6\bar{p}; v_6 = 7s, 6d, 6f, 6g, 7p; \bar{v}_6 = 7\bar{s}, 6\bar{d}, 6\bar{f}, 6\bar{g}, 7\bar{p}; \bar{v}_7 = 8\bar{s}, 7\bar{d}, 7\bar{f}, 7\bar{g}, 8\bar{p}$ .

<sup>c</sup>Denote the target states formed by spectroscopy orbitals, represent the physical states observed in the spectrum.

<sup>d</sup>Denote the physical target states used in corresponding basis set.

<sup>e</sup>Denote other quasistates involve pseudo-orbitals.

<sup>f</sup>Configurations formed by spectroscopy orbitals and pseudo-orbitals in corresponding basis set.  $AO^2$  denote the  $n_1 l_1 n_2 l_2$  and  $n_1 l_1^2$  types of configurations.  $AO^3$  denote the  $n_1 l_1 n_2 l_2 n_3 l_3, n_1 l_1 n_2 l_2^2$ , and  $n_1 l_1^3$  types of configurations.

derivative boundary matrix  $R(E)$ . Therefore, within the reaction zone the electron correlations for the ( $N + 1$ )-electron system including the target Na and a colliding electron are calculated adequately by variational method [19]. The wave function  $\Psi$  for the ( $N + 1$ )-electron system of eigenenergy  $E$  within the reaction zone are expanded as:

$$\Psi = \sum_k A_{E_k} \Psi_k, \quad (1)$$

where  $\Psi_k$  are the energy-independent bases, which are expanded by the following way:

$$\Psi_k = A \sum_{ij} a_{ijk} \Phi_i \frac{1}{r_{N+1}} u_{ij}(r_{N+1}) + \sum_j b_{jk} \phi_j, \quad (2)$$

where  $A$  is the antisymmetrization operator which accounts for the electron exchanges between the target electrons and the colliding electron.  $\Phi_i$  are the channel wave functions obtained by coupling the  $N$ -electron target wave functions with the angular momentum and spin of the colliding electron.  $u_{ij}$  are the continuum orbitals.  $\phi_j$  are ( $N + 1$ )-electron wave functions formed from the bound-type orbitals to ensure the completeness of the total wave functions and take account of the electron correlations within the reaction zone. The coefficients  $a_{ijk}$  and  $b_{jk}$  are obtained by diagonalizing the Hamiltonian matrix of the ( $N + 1$ )-electron system. Using the  $R$ -matrix method, we can accurately calculate the interactions between the  $N$ -electron target and the colliding electron in various channels within the reaction zone.

In this work, based on multiconfiguration self-consistent field (MCSCF) calculation strategies [20], we use CIVPOL code [21] to optimize four sets of high-quality target orbital bases where polarized pseudo-orbitals [22–24] are included, by which we can take into account the static polarization effects between the scattered electron and the target electrons adequately. The differences between the four sets of bases are

mainly the number of spectroscopy orbitals used to describe the physical target states which correspond to the physical states observed in the spectrum. The orbitals in each set are listed in Table I. More specifically, the four sets of orbital bases classified by manifold of effective quantum number  $\nu$  are constructed from atomic orbitals including spectroscopy orbitals (labeled as  $nl$  and with fixed number of radial nodes, i.e.,  $n-l-1$ ) and pseudo-orbitals (labeled as  $n\bar{l}$  and without restriction of radial nodes). For  $\nu \leq n_p$ , where  $n_p = 3, \dots, 6$  for basis sets  $p = 1, \dots, 4$  respectively, the orbitals are optimized as spectroscopy orbitals with the configurations generated with single excitation from  $3s^1$  only. In order to consider the dynamic polarization correlations adequately, we further optimize the  $\nu = n_p + 1$  manifold orbitals as polarized pseudo-orbitals with the configurations created by single excitations respectively from core  $2p^6$  and valence  $3s^1$ . The calculated energy levels of the corresponding physical target states of the four sets are all in good agreement with the experimental values [25] within 1%. As an example, using the orbitals of Set 4, our calculated lowest 19 energy levels of target (i.e., Na) are shown in Table II. Such agreement demonstrates that the electron correlations of target are taken into account adequately. Using these sets of “quasicomplete” bases, we can construct configuration interaction (CI) wave functions of the target states with the configurations generated by single excitations respectively from core  $2p^6$  and valence  $3s^1$ . Based on these wave functions, we carefully choose four sets of target terms respectively to calculate the collision cross sections. The highest target state excitation energy of each set is larger than 2.89 au. As shown in Table I, Set 1 includes five physical states (with effective quantum number  $\nu \leq 3$ ) and 26 other pseudostates which involve pseudo-orbitals, Set 2 includes 9 physical states (with  $\nu \leq 4$ ) and 42 other states, Set 3 includes 14 physical states (with  $\nu \leq 5$ ) and 41 other states while Set 4 includes 19 physical states (with  $\nu \leq 6$ ) and 43 other states. By using these sets of target, we can systematically examine

TABLE II. Our calculated lowest 19 energy levels of Na (in eV unit) relative to the energy level of ground state Na[ $2p^63s^1$ ]  $^2S^e$  using basis set 4.

No.	Physical target state	This work	NIST data [25]	$\Delta^a$
1	$2p^63s^1\ ^2S^e$	–	–	–
2	$2p^63p^1\ ^2P^o$	2.120 123 79	2.104 550 266	0.74%
3	$2p^64s^1\ ^2S^e$	3.171 185 44	3.191 535 405	–0.64%
4	$2p^63d^1\ ^2D^e$	3.593 495 87	3.617 178 752	–0.65%
5	$2p^64p^1\ ^2P^o$	3.738 819 42	3.753 537 088	–0.39%
6	$2p^65s^1\ ^2S^e$	4.093 060 03	4.116 595 446	–0.57%
7	$2p^64d^1\ ^2D^e$	4.258 547 37	4.283 742 686	–0.59%
8	$2p^64f^1\ ^2F^o$	4.261 839 97	4.288 477 79	–0.62%
9	$2p^65p^1\ ^2P^o$	4.323 855 21	4.345 009 152	–0.49%
10	$2p^66s^1\ ^2S^e$	4.486 267 65	4.509 889 087	–0.52%
11	$2p^65d^1\ ^2D^e$	4.566 37 86	4.592 235 937	–0.56%
12	$2p^65f^1\ ^2F^o$	4.568 215 38	4.594 826 859	–0.58%
13	$2p^65g^1\ ^2G^e$	4.568 310 62	4.595 061 203	–0.58%
14	$2p^66p^1\ ^2P^o$	4.600 665 21	4.624 419 867	–0.51%
15	$2p^67s^1\ ^2S^e$	4.687 361 37	4.713 163 429	–0.55%
16	$2p^66d^1\ ^2D^e$	4.733 498 64	4.759 686 583	–0.55%
17	$2p^66f^1\ ^2F^o$	4.734 614 31	4.761 240 566	–0.56%
18	$2p^66g^1\ ^2G^e$	4.734 668 74	4.761 377 701	–0.56%
19	$2p^67p^1\ ^2P^o$	4.753 757 67	4.778 647 708	–0.52%

<sup>a</sup>Percentage difference between our calculation results and the NIST data [25],  $(E_{\text{theor}} - E_{\text{NIST}})/E_{\text{NIST}}$ .

the convergence of the scattering calculations and elucidate the influence of the Rydberg states to the collision cross sections. For each angular momentum  $l$  of the scattering electron, we choose more than 60 Lagrange-orthogonalized continuum orbitals. The highest orbital energies of them are larger than 3.5 au. Furthermore, the total wave functions of  $(N+1)$ -electron system of the inner region are constructed according to Eq. (2). The  $(N+1)$ -electron configurations used in the calculations are also shown in Table I, where all configurations generated by single excitations respectively from the core  $2p^6$  and double excitation from valence  $3s^2$  of each set are adopted in order to consider the electron correlations within the reaction zone adequately and avoid pseudo-resonance, which will be discussed later.

In the outer region, the wave function of the colliding electron satisfies the boundary conditions at infinity:

$$F_{ij}(r) \underset{r \rightarrow \infty}{\sim} \begin{cases} k_i^{-1/2} [\sin \theta_i(r) \delta_{ij} + \cos \theta_i(r) K_{ij}], & \text{open channels,} \\ \exp[-\varphi_i(r)] \delta_{ij}, & \text{closed channels,} \end{cases} \quad (3)$$

where  $k_i$  is the wave number of colliding electron and

$$\theta_i(r) = k_i r - \frac{1}{2} l_i \pi - \eta_i \ln 2k_i r + \arg \Gamma(l_i + 1 + i\eta_i), \quad (4)$$

$$\eta_i = -\frac{z}{k_i}, \quad (5)$$

$$\varphi_i(r) = |k_i| r - \frac{z}{|k_i|} \ln(2|k_i| r), \quad (6)$$

where  $z$  is the residual target charge.  $K$  is the reaction matrix, from which we obtain the transition matrix by:

$$T = \frac{2iK}{1 - iK}. \quad (7)$$

Here  $K$  and  $T$  are all diagonal with respect to the total angular momentum  $L$ , total spin  $S$ , and parity  $\Pi$  of the  $(N+1)$ -electron system and independent of the projections of  $L$  and  $S$  on the quantization axis. From the  $T$  matrix we can construct scattering amplitudes, cross sections, or other scattering quantities [26]. The differential cross section for a transition from an initial target state denoted by  $\alpha_i \tilde{L}_i \tilde{S}_i$  to a final target state denoted by  $\alpha_j \tilde{L}_j \tilde{S}_j$ , where  $\alpha_i$  and  $\alpha_j$  represent the additional quantum numbers necessary to completely define the target states, is:

$$\begin{aligned} \frac{d\sigma}{d\Omega}(\alpha_i \tilde{L}_i \tilde{S}_i \rightarrow \alpha_j \tilde{L}_j \tilde{S}_j | \theta) &= \frac{k_j}{2k_i} |f_{ij}|^2 \\ &= \sum_{\lambda} A_{\lambda}(\alpha_i \tilde{L}_i \tilde{S}_i \rightarrow \alpha_j \tilde{L}_j \tilde{S}_j) P_{\lambda}(\cos \theta), \end{aligned} \quad (8)$$

where  $f_{ij}$  is the scattering amplitude and

$$\begin{aligned} A_{\lambda}(\alpha_i \tilde{L}_i \tilde{S}_i \rightarrow \alpha_j \tilde{L}_j \tilde{S}_j) &= \frac{1}{8k_i^2 (2\tilde{L}_i + 1)(2\tilde{S}_i + 1)} \sum_{l_i l_i' l_j' S_i} i^{l_i - l_j + l_i' - l_j'} (-1)^{j_i + \lambda} \\ &\times (2j_i + 1) \langle l_i l_i' 00 | \lambda 0 \rangle \langle \lambda 0 | l_j l_j' 00 \rangle W(l_i l_j l_i' l_j'; j_i \lambda) \\ &\times M_{l_i l_i'}^{S_i j_i}(\alpha_i \tilde{L}_i \tilde{S}_i \rightarrow \alpha_j \tilde{L}_j \tilde{S}_j) M_{l_i l_i'}^{S_i j_i}(\alpha_i \tilde{L}_i \tilde{S}_i \rightarrow \alpha_j \tilde{L}_j \tilde{S}_j), \end{aligned} \quad (9)$$

where we define:

$$\begin{aligned} M_{l_i l_i'}^{S_i j_i}(\alpha_i \tilde{L}_i \tilde{S}_i \rightarrow \alpha_j \tilde{L}_j \tilde{S}_j) &= \sqrt{(2l_i + 1)(2l_i' + 1)(2S_i + 1)} \\ &\times \sum_{L\pi} (-1)^L (2L + 1) W(l_i l_i' l_j \tilde{L}_j; L j_i) \\ &\times T_{(l_i l_i')}^{LS\pi}(\alpha_i \tilde{L}_i \tilde{S}_i \rightarrow \alpha_j \tilde{L}_j \tilde{S}_j). \end{aligned} \quad (10)$$

Here  $k_i^2$  is the energy of the incident electron;  $l_i$  and  $l_j$  are the angular momenta of incident and scattered electrons;  $j_i = l_j - l_i = \tilde{L}_i - \tilde{L}_j$  is the angular momentum transferred during the collision;  $P_{\lambda}(\cos \theta)$  are the Legendre polynomials and  $W(abcd; ef)$  is a Racah coefficient defined in Ref. [27]. The total cross section for this transition is given by:

$$\sigma_{(\alpha_i \tilde{L}_i \tilde{S}_i) \rightarrow (\alpha_j \tilde{L}_j \tilde{S}_j)} = 4\pi A_0(\alpha_i \tilde{L}_i \tilde{S}_i \rightarrow \alpha_j \tilde{L}_j \tilde{S}_j), \quad (11)$$

which can be expressed as the summation of infinite partial cross sections:

$$\sigma_{(\alpha_i \tilde{L}_i \tilde{S}_i) \rightarrow (\alpha_j \tilde{L}_j \tilde{S}_j)} = \sum_{LS\pi} \sigma_{(\alpha_i \tilde{L}_i \tilde{S}_i) \rightarrow (\alpha_j \tilde{L}_j \tilde{S}_j)}^{LS\pi}, \quad (12)$$

where the partial cross section for this transition is:

$$\begin{aligned} \sigma_{(\alpha_i \tilde{L}_i \tilde{S}_i) \rightarrow (\alpha_j \tilde{L}_j \tilde{S}_j)}^{LS\pi} &= \frac{\pi}{2k_i^2} \sum_{l_i, l_j} \frac{(2L + 1)(2S + 1)}{(2\tilde{L}_i + 1)(2\tilde{S}_i + 1)} \\ &\times |T_{l_i, l_j}^{LS\pi}(\alpha_i \tilde{L}_i \tilde{S}_i, \alpha_j \tilde{L}_j \tilde{S}_j)|^2. \end{aligned} \quad (13)$$

Based on the partial cross section method, we calculated the elastic and inelastic scattering cross sections of Na impacted by low-energy electron using the FARM code [28]. Figures 1–2 show the partial cross sections excited from ground state to the final states of  $3s$  and  $3p$  at three low incident energies (in eV): 3.4, 4.1, 5.4. In Fig. 1, the elastic collision partial cross sections for  $3s$  decrease rapidly with the increasing

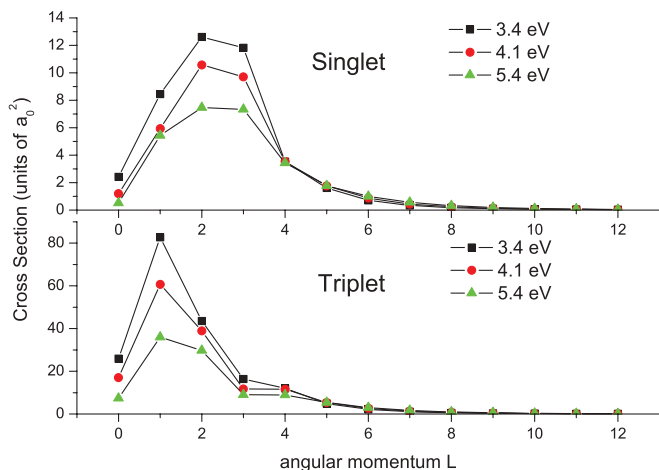


FIG. 1. (Color online) The elastic partial cross sections for various  $L, S$ .

total angular momentum  $L$ . In Fig. 2, the inelastic collision partial cross sections for optical allowed  $3s$ - $3p$  transitions also decrease but more slowly with the increasing total angular momentum. Based on a picture of virtual photon [29], the optical allowed collision excitation can be viewed as the interaction between virtual photon sources and the target with various impact parameters (corresponding to various  $L$ ), hence the contributions of high partial waves become larger. Because of more partial-wave contributions, features of resonances for specific partial waves and incident energies become less prominent, which are shown in Fig. 6 later. Therefore, we can conclude that, at low incident energies, the high partial cross sections decrease with the increasing angular momentum. According to this conclusion, since the contributions of infinite high partial cross sections in the total cross sections are negligible, we only need to calculate the contributions of finite low partial cross sections at low incident energies. The partial waves used are adequate for all calculations of cross sections in present work.

In order to verify the precision of our partial-wave calculations, we should note that there exists a bound state for

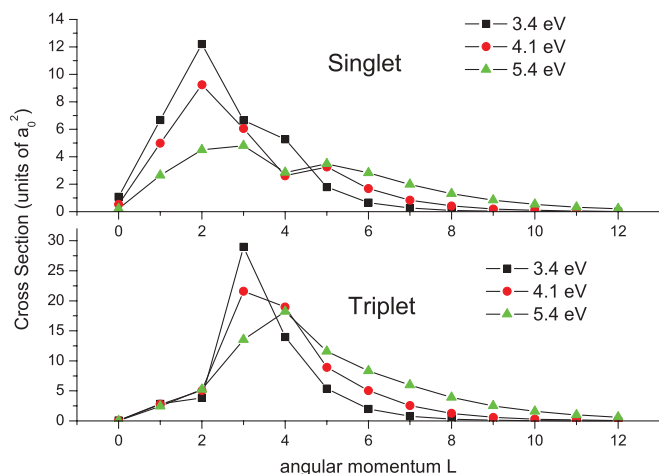


FIG. 2. (Color online) The  $3s$ - $3p$  partial cross sections for various  $L, S$ .

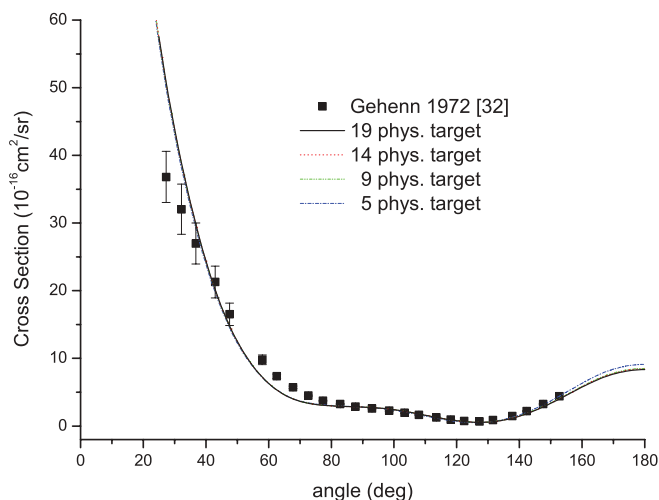


FIG. 3. (Color online) The elastic differential cross section excitation at 2.1 eV.

$^1S^e$  partial wave, the affinity of which can be accurately measured by the laser spectroscopy experiment. Since the  $R$ -matrix method treats the bound states and adjacent continua on equal footing, the precision of the calculated bound states energies can then be used as a precise criterion for evaluating the accuracy of the continuum states phase-shift calculations. Our calculated electron affinity of  $\text{Na}^- [2p^6 3s^2] ^1S^e$  is 0.541 eV, which is in good agreement with the experimental value [30] of 0.548 eV within about 1%. The precision of the affinity calculation can even achieve a higher accuracy if the polarization of the target is described better. The calculation of the affinity will be reported elsewhere [31]. Nevertheless, such precision is already adequate for scattering cross-section calculations and it is demonstrated that the electron correlations of the  $(N+1)$ -electron system have been taken into account adequately. We could anticipate the calculation precision of other partial waves should be at the same level.

Our calculation results of various cross sections are shown in Figs. 3–9. The cross sections calculated by 5 physical target states are shown by a dash-dotted blue line; the cross sections calculated by 9 physical target states are shown by a dash-double-dotted green line; the cross sections calculated by 14 physical target states are shown by the dotted red line while the cross sections calculated by 19 physical target states are shown by the solid black line. The differential elastic cross section for the ground state  $3s$  at 2.1 eV (below the next excitation threshold  $3p$ ) is shown in Fig. 3. The calculated cross sections using the four sets of “quasicomplete” bases of the target are consistent with each other and in good agreement with experimental measurements [32]. The total cross section including the dominant elastic cross section as well as various excitation cross sections (with incident energies above excitation threshold), at incident energy ranging from 0 to 5.4 eV is shown in Fig. 4. It needs to be noted that, for sodium, the experimental total cross section is the most accurate absolute measurement of scattering cross sections, because no cascade corrections [7] are needed. As shown in Fig. 4, our calculated cross sections using the four sets of “quasicomplete” bases of the target are consistent

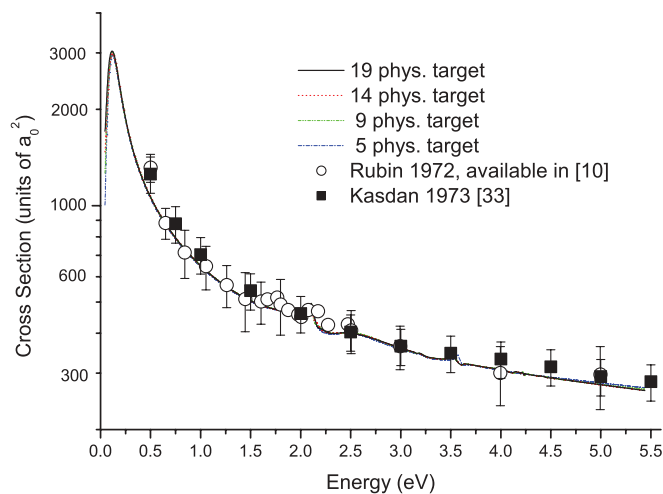


FIG. 4. (Color online) Total cross section for scattering of electrons by sodium.

with each other and in good agreement with experimental measurements [10,33], which demonstrates the good quality of our calculations. The differential cross section for  $3s$ - $3p$  excitation at 2.6 eV (below the next excitation threshold  $4s$ ) is shown in Fig. 5. As shown in Fig. 5, the calculated cross sections using the four sets of “quasi-complete” bases of the target are consistent with each other and in agreement with experimental measurements [34]. The experimental cross section has data only in small scattering angles; the cross section of large scattering angles deserves further experimental studies. Note that our calculated integrated cross sections for  $3s$ - $3p$  at this incident energy are also in good agreement with absolute experimental measurement [9], which is shown in Fig. 6.

Figures 6–9 are our calculated integrated collision excitation cross sections of Na, from  $3s$  to  $3p$ ,  $4s$ ,  $3d$ , and  $4p$  states respectively. The available experimental cross sections are also shown in these figures. Since the line widths of the electron beams used in the experiment are about 750 meV [9], in order to compare with the experiment data more clearly, we fold

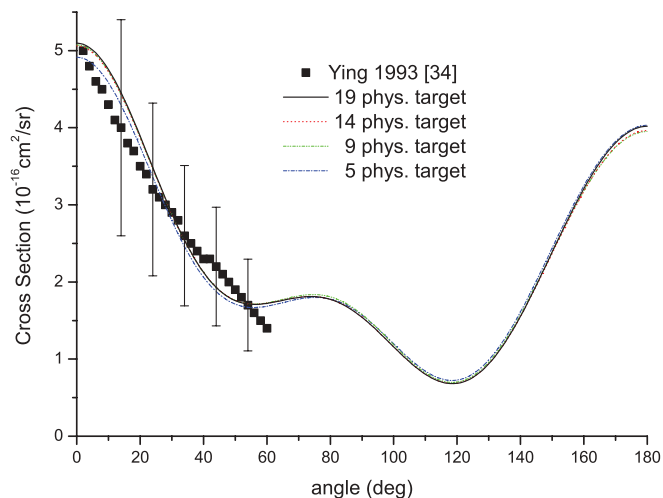


FIG. 5. (Color online) The differential cross section for  $3s$ - $3p$  excitation at 2.6 eV.

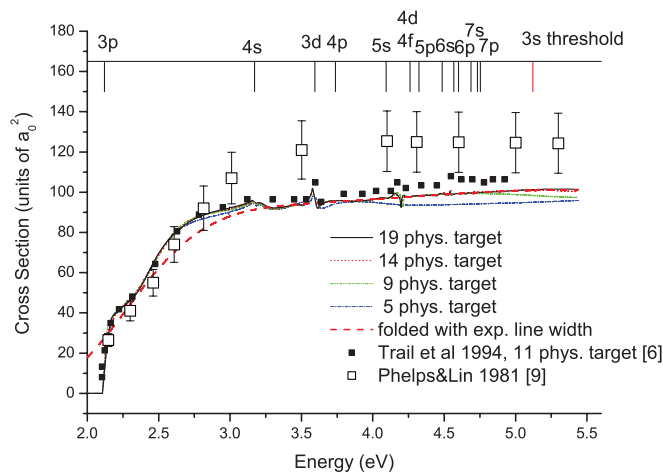


FIG. 6. (Color online) The  $3s$ - $3p$  excitation cross sections.

our calculated cross sections with the experimental line width, which are shown as the dashed red line in Figs. 6–9. Note that the experimental measurement method for excitation cross sections is the optical method [7], in which the cross sections are obtained from the fluorescence signal of the excited states. Therefore, the most important issue for experimental measurements is to determine the population of collision excitation, i.e., to determine cascade corrections [7].

For the optical allowed  $3s$ - $3p$  excitation cross section, as shown in Fig. 6, our calculation results are in excellent agreement with previous 11 physical target states calculation results [6] with the incident energies lower than about 3.6 eV. For the incident energies larger than 3.6 eV, our results are a little smaller than previous theoretical results [6]. Compared with experimental results, for the incident energies lower than about 3 eV (below  $4s$  threshold), our calculation results are in agreement with experimental data [9]. Because no cascade corrections are needed for this energy region. However, our calculation results and other theoretical results are significantly smaller than the experimental data at incident energies larger than 3 eV. These large deviations at high incident energies should be due to the experimental difficulties, most probably the uncertainties of cascade corrections [7] in the measurements of excitation cross sections, because the main contribution of cascade corrections for  $3p$  comes from the dipole transition of  $4s$  and  $3d$ . As can be seen

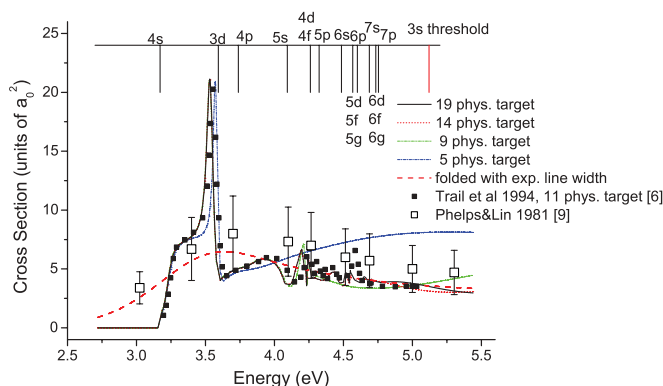
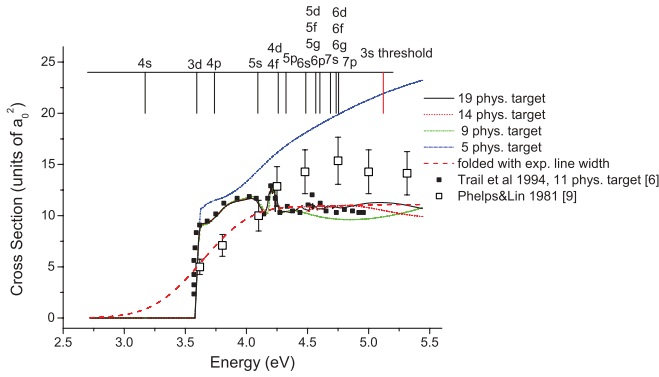
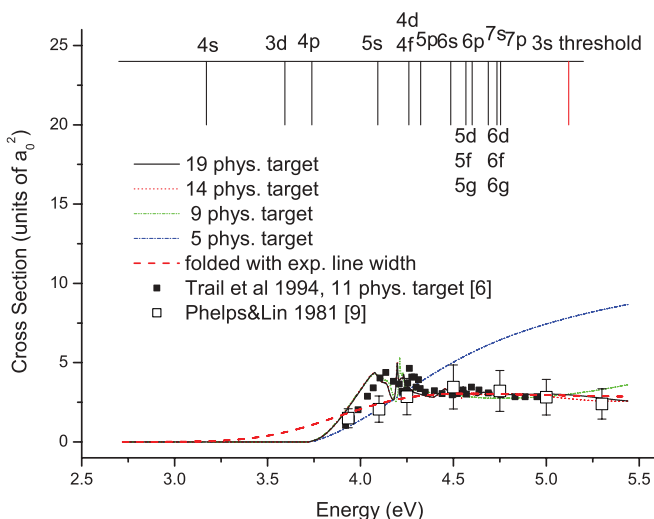


FIG. 7. (Color online) The  $3s$ - $4s$  excitation cross sections.

FIG. 8. (Color online) The  $3s$ - $3d$  excitation cross sections.

from Fig. 7 and 8, the excitation cross sections of  $4s$  and  $3d$  are not small. So the uncertainties of cascade corrections are large for  $3s$ - $3p$  excitation cross sections at the incident energies above these thresholds. Considering the uncertainties of cascade corrections, our calculation results are in marginally agreement with experimental results. However, the more precision experimental measurements are expected. The cross sections calculated by our four sets of “quasicomplete” bases of the target, as shown in Fig. 6, exhibit convergent properties when the physical targets increase. The amplitudes of the resonance structures are very small, which can be understood from the picture of virtual photon [29]. Because the electron excitation is nearly equivalent to the interaction between virtual photon sources and the target with various impact parameters (corresponding to various  $L$ ), the contributions of high partial waves become larger and the features of resonances for specific partial waves and incident energies become less prominent. From Fig. 6 we can also see that the amplitudes of resonance structures decrease with respect to the effective quantum number  $\nu$  of the Rydberg target states, which will be discussed below.

For optical forbidden  $3s$ - $4s$  excitation cross section, as shown in Fig. 7, our calculated cross sections are in good agreement with the experimental measurements within the experimental error bars. Because the small excitation cross

FIG. 9. (Color online) The  $3s$ - $4p$  excitation cross sections.

section of  $4p$  (as shown in Fig. 9) made the cascade corrections small for the  $3s$ - $4s$  cross section. From the calculated cross sections, we can see that the contribution of resonance structure is very large. Unlike the  $3s$ - $3p$  excitation cross section, there are some significant differences between the cross section calculated by 5 physical target states and by the other 3 target bases sets with more physical target states, which illustrates that the 5 target physical states are not sufficient for the cross section calculations in this energy region. The differences between the cross sections of the other 3 target bases sets are only in the energy region above the thresholds of the newly added physical target states, the contributions of which to the cross sections become smaller and smaller and almost negligible at  $\nu > 6$ . This result can be understood from the point that when the incident energies increase, more and more channels are opened, hence the contribution of a specific channel in total resonance structure becomes smaller and smaller. It is interesting to note that there are some deviations from previous 11 physical target states calculation results [6]. More specifically, our calculated results are in good agreement with other theoretical calculations in low excitation energies. But for the higher excitation energies, the previous calculations are a little larger than our work and some resonance structures may be pseudoresonance, especially the resonance structure at 4.6 eV (i.e., the thresholds of  $\nu_5$  manifold). Because the amplitude of this resonance structure in previous 11 physical target states calculation is much larger than our 14 and 19 physical target states calculations, while our two sets of calculations are consistent with each other. From our experience, some pseudoresonances are relevant to the balance between the configurations of the target states and the  $(N + 1)$ -electron bound type configurations used to ensure the completeness of the total wave functions. In fact we have included all types of  $(N + 1)$ -electron configurations excited with the same excitation level of the target states to avoid such pseudoresonances. If we omit some  $(N + 1)$ -electron bound-type configurations in the calculations, especially those with the type of  $2p^5 n_1 l_1^2 n_2 l_2$  and  $2p^5 n_1 l_1^3$ , some pseudoresonances may arise.

For the optical forbidden  $3s$ - $3d$  excitation cross section, as shown in Fig. 8, there are some significant differences between the cross sections calculated by 5 physical target states and the other 3 target bases sets with more physical target states. The differences between the cross sections of the other 3 bases sets are only in the energy region above the newly added physical target states. Their contributions to the cross sections become smaller and smaller and can be almost neglected at  $\nu > 6$ . Our 14 and 19 physical target states calculation results are in excellent agreement with 11 physical target states calculation results [6] at the incident energies lower than about 4.4 eV. For the incident energies larger than 4.4 eV, our results are a little larger than previous theoretical results [6]. Note that the amplitude of the resonance structure at 4.6 eV (i.e., the thresholds of  $\nu_5$  manifold) of previous 11 physical target states calculation is also much larger than our 14 and 19 physical target states calculations. Compared with experimental results, for the incident energies lower than about 4.2 eV (below  $4f$  threshold), our calculation results are in agreement with experimental data [9]. However, our calculation results and other theoretical results are significantly

smaller than the experimental ones at incident energies larger than 4.2 eV. These large deviations at high incident energies most probably result from the uncertainties of cascade corrections of  $4f$ , because the oscillator strength for  $4f$  is much larger than  $4p$  and the excitation cross section for  $4p$  is small.

For the  $3s$ - $4p$  excitation cross section, as shown in Fig. 9, the convergence properties of the cross sections calculated by 4 sets of “quasicomplete” bases of the target are the same as other excitation cross sections. There are some deviations between our calculation results and previous 11 physical target states calculation results [6], which may indicate that the number of physical target states used in previous calculations is not sufficient for this higher excitation cross section. Compared with experimental results, our calculation results are in agreement with experimental one [9] for all incident energies below 5.4 eV. Because the  $3s$ - $4p$  excitation cross section is very small, the influence of cascade correction becomes less prominent.

### III. CONCLUSIONS

Finally, we would like to conclude with the following remarks. In present work, we use the  $R$ -matrix method to calculate the collision cross sections of sodium with high precision from ground state to the first four excited states at the incident energy range of 0–5.4 eV (above the  $3s$  ionization threshold) systematically. The precision of our scattering calculations can be verified by the accuracy of the  $\text{Na}^-$  affinities calculation which is about 1%. By using 4 sets of high-quality target orbital bases including polarized pseudo-orbitals, as shown in Tables I and II, we can examine the convergence of the scattering calculations. Our calculation results are generally in good agreement with experimental measurements and other theoretical calculations. More specifically, for the elastic differential cross section of  $3s$ , differential cross section of  $3s$ - $3p$  at low incident energies and the total cross section from  $3s$ , where no cascade corrections for experimental data are needed, our calculation cross sections show excellent agreement with experimental data, as shown in Figs. 3–5. For the excitation cross sections of  $3s$ - $3p$ ,  $3s$ - $4s$ ,  $3s$ - $3d$ , and  $3s$ - $4p$ , our calculation cross sections are in good agreement with experimental data at low incident energies where the contribution of cascade corrections is very small. However, at higher incident energies, our calculation results are lower than the experimental measurements, especially for  $3s$ - $3p$  and  $3s$ - $3d$  excitation cross sections, as shown in Figs. 6–9. Such deviations should be owing to the difficulties in deciding cascade corrections in the measurements of excitation cross sections, which deserves further experimental and theoretical studies. Furthermore, using such 4 sets of high-quality target orbital bases, we can also elucidate the influence of the Rydberg states on the collision cross sections, especially for the optical forbidden excitations. As shown in Figs. 6–9, the amplitudes of resonance structures decrease with the effective quantum number  $\nu$ , which represents the Rydberg states involved. It means that the resonance structures in these cross sections at higher incident energies are not important. Therefore, it needs to include only finite physical target states in practical calculations. This result

also demonstrates that the cross sections obtained by the partial wave expansion methods valid at low energy could be interfaced with the cross sections obtained by the first Born approximation method valid at high energy [18], which would be very powerful for providing cross-section data with high quality in related scientific fields. This is because partial wave expansions are only appropriate for low-energy region. For intermediate-energy and high-energy regions, the scattering amplitudes  $f$  should be calculated as a whole. At high electron energies as Born approximation is valid, various cross sections can be readily calculated, i.e.,  $f \cong f^{\text{Born}}$ . Note that,  $f^{\text{Born}} = \sum_{LS\pi} f_{LS\pi}^{\text{Born}}$  is the summation of infinite partial wave contributions. The expression for the Born partial scattering amplitude  $f_{LS\pi}^{\text{Born}}$  can be found in Ref. [35]. At intermediate energy region the Born approximation cannot be applied directly. However, as the angular momentum  $L$  increases, the exact partial scattering amplitude  $f_{LS\pi}$  converges to the corresponding Born partial scattering amplitude  $f_{LS\pi}^{\text{Born}}$  [36] because the large centrifugal potential will exclude the scattering electron outside the reaction zone. Therefore starting from Born approximations [18], the scattering amplitude  $f$  can be calculated by  $f = f^{\text{Born}} + \Delta f$ , where the correction function  $\Delta f$  can be calculated by partial-wave expansions involving only a finite number of penetrating partial waves (i.e., low angular momentums). More specifically, we can define an  $L_{\text{max}}$ , beyond which all  $\Delta f_{LS\pi}$  with  $L \geq L_{\text{max}}$  satisfy the relation  $|\Delta f_{LS\pi}| < \delta$ , where  $\delta$  is an appropriate convergence criterion. Then  $\Delta f = \sum_{S\pi, L=0}^{S\pi, L=L_{\text{max}}} \Delta f_{LS\pi}$ . For the intermediate-energy region, when the incident energy is above the ionization threshold, there will be no resonance structures at all; when the incident energy is lower than the ionization threshold, our calculation result shows the resonance structures can be neglected in such an energy region. Therefore the correction functions for the transitions between the lower excited targets were expected to be smoothly varying functions. In fact, various authors [37,38] have already made use of empirical quasiuniversal scaling factors between the Born and “exact” cross sections and obtain some cross sections in agreement with the experimental and more rigorous theoretical results. Nevertheless, how to efficiently interface the cross sections of low incident energies and high incident energies still deserves further studies. Using the scattering matrices calculated in present work, we can further calculate the quantities such as angular distribution and spin polarization to meet the requirements of “complete experiments.” However, this is beyond the scope of present article, which deserves further studies.

### ACKNOWLEDGMENTS

This work is supported by Ministry of Science and Technology and Ministry of Education of China, the Key grant Project of Chinese Ministry of Education (No. 306020), the National Natural Science Foundation of China (Grant Nos. 10734040, 10933001, 10804012), the National High-Tech ICF Committee in China and the Yin-He Super-computer Center, Institute of Applied Physics and Mathematics, Beijing, China, and National Basic Research Program of China (Grant No. 2006CB921408).

- [1] L. G. Christophorou, *Atomic and Molecular Radiation Physics* (John Wiley & Sons Ltd, New York, 1971).
- [2] J. D. Lindl *et al.*, *Phys. Plasmas* **11**, 339 (2004).
- [3] A. Dalgarno, *Adv. At., Mol. Phys.* **15**, 37 (1979).
- [4] T. R. Kallman and P. Palmeri, *Rev. Mod. Phys.* **79**, 79 (2007).
- [5] P. Beiersdorfer, *Annu. Rev. Astron. Astrophys.* **41**, 343 (2003).
- [6] W. K. Trail, M. A. Morrison, H. L. Zhou, B. L. Whitten, K. Bartschat, K. B. MacAdam, T. L. Goforth, and D. W. Norcross, *Phys. Rev. A.* **49**, 3620 (1994).
- [7] C. C. Lin and J. B. Boffard, *Adv. At., Mol. Phys.* **51**, 385 (2005).
- [8] E. A. Enemark and A. Gallagher, *Phys. Rev. A.* **6**, 192 (1972).
- [9] J. O. Phelps and C. C. Lin, *Phys. Rev. A* **24**, 1299 (1981).
- [10] D. L. Moores and D. W. Norcross, *J. Phys. B* **5**, 1482 (1972).
- [11] P. G. Burke, A. Hibbert, and W. D. Robb, *J. Phys. B* **4**, 153 (1971).
- [12] K. A. Berrington, P. G. Burke, J. J. Chang, A. T. Chivers, W. D. Robb, and K. T. Taylor, *Comput. Phys. Commun.* **8**, 149 (1974).
- [13] K. A. Berrington, P. G. Burke, M. Dourneuf, W. D. Robb, K. T. Taylor, and L. Voky, *Comput. Phys. Commun.* **14**, 367 (1978).
- [14] K. A. Berrington, P. G. Burke, K. Butler, M. J. Seaton, P. J. Storey, K. T. Taylor, and Y. Yan, *J. Phys. B* **20**, 6379 (1987).
- [15] L. Voky, H. E. Saraph, W. Eissner, Z. W. Liu, and H. P. Kelly, *Phys. Rev. A* **46**, 3945 (1992).
- [16] K. A. Berrington and A. E. Kingston, *J. Phys. B* **20**, 6631 (1987).
- [17] K. A. Berrington, W. B. Eissner, and P. H. Norrington, *Comput. Phys. Commun.* **92**, 290 (1995).
- [18] X. Y. Han and J. M. Li, *Phys. Rev. A* **74**, 062711 (2006); X. Y. Han, Y. M. Li, H. Zhang, J. Yan, J. M. Li, and L. Voky, *ibid.* **78**, 052702 (2008).
- [19] U. Fano and C. M. Lee (J. M. Li), *Phys. Rev. Lett.* **31**, 1573 (1973).
- [20] B. Qing, C. Cheng, X. Gao, X. L. Zhang, and J. M. Li, *Acta. Phys. Sin.* **59**, No. 7, in publish (2010) (in Chinese).
- [21] Hibbert A., *Comput. Phys. Commun.* **9**, 141 (1975).
- [22] J. Yan, Y. Z. Qu, L. Voky, and J. M. Li, *Phys. Rev. A* **57**, 997 (1998).
- [23] Y. L. Peng, M. S. Wang, X. Y. Han, and J. M. Li, *Chin. Phys. Lett.* **21**, 1723 (2004).
- [24] Y. L. Peng, M. S. Wang, X. Y. Han, and J. M. Li, *J. Phys. B* **38**, 3825 (2005).
- [25] Y. Ralchenko, A. E. Kramida, J. Reader, and NIST ASD Team (2008). NIST Atomic Spectra Database (version 3.1.5) [online]. Available: [http://physics.nist.gov/PhysRefData/ASD/levels\\_form.html](http://physics.nist.gov/PhysRefData/ASD/levels_form.html) [2010, January 7] National Institute of Standards and Technology, Gaithersburg, MD.
- [26] S. A. Salvini, *Comput. Phys. Commun.* **27**, 25 (1982).
- [27] D. M. Brink and G. R. Satchler, *Angular Momentum*, 2nd ed. (Clarendon Press, Oxford, 1968).
- [28] V. M. Burke and C. J. Noble, *Comput. Phys. Commun.* **85**, 471 (1995).
- [29] J. D. Jackson, *Classical Electrodynamics*, 3rd ed. (John Wiley & Sons Ltd., New York, 1999), Chap. 15.
- [30] T. A. Patterson, H. Hotop, A. Kasdan, D. W. Norcross, and W. C. Lineberger, *Phys. Rev. Lett.* **32**, 189 (1974).
- [31] X. Gao and J. M. Li, *J. Phys.: Conf. Ser.* **194**, 022002 (2009). (Proceedings of the XXVI International Conference on Photonic, Electronic, and Atomic Collisions).
- [32] W. Gehenn and E. Reichert, *Z. Phys.* **254**, 28 (1972).
- [33] A. Kasdan, T. M. Miller, and B. Bederson, *Phys. Rev. A* **8**, 1562 (1973).
- [34] C. H. Ying, F. Perales, L. Vuskovic, and B. Bederson, *Phys. Rev. A* **48**, 1189 (1993).
- [35] M. J. Seaton, *Proc. Phys. Soc.* **77**, 184 (1961); J. Lawson, W. Lawson and M. J. Seaton, *ibid.* **77**, 192 (1961).
- [36] X. Pan, *Phys. Rev. Lett.* **66**, 2972 (1991).
- [37] Y. Z. Qu, J. G. Wang, X. M. Tong and J. M. Li, *Chin. Phys. Lett.* **12**, 581 (1995); J. M. Li, *Acta. Phys. Sin.* **29**, 419 (1980) (in Chinese); B. G. Tian and J. M. Li, *ibid.* **35**, 203 (1986) (in Chinese).
- [38] Y. K. Kim, *Phys. Rev. A.* **64**, 032713 (2001); **65**, 022705 (2002).